ELSEVIER

Journal of Power Sources 92 (2001) 149–156

JOURNAL OF POWER SOURCES

www.elsevier.com/locate/jpowsour

Effect of fluorination on the lanthanum-doped AB_2-type metal hydride electrodes

H.Y. Park[a,*], W.I. Cho[b], B.W. Cho[b], S.R. Lee[a], K.S. Yun[b]

[a]*Department of Metallurgical Engineering, Korea University, Seoul 136-701, South Korea*
[b]*Battery and Fuel Cell Research Center, Korea Institute of Science and Technology, Seoul 136-791, South Korea*

Received 29 February 2000; received in revised form 8 May 2000; accepted 28 May 2000

Abstract

The effect of fluorination on the surface of an AB_2-type hydrogen-storage alloy with the composition $Zr_{0.7}Ti_{0.3}V_{0.4}Mn_{0.4}Ni_{1.2}$ is investigated. Electron probe microanalysis (EPMA), scanning electron microscopy (SEM), Auger electron spectroscopy (AES), and X-ray diffraction (XRD) techniques show that the fluorinated AB_2-type alloys have a unique surface morphology and high reactivity with a protective film. The treatment is found to be effective when lanthanum is incorporated in the alloy. The cycle-life of the metal hydride (MH) electrode increases significantly as a result of a decrease in the overpotential by electrode polarization. The degradation rate of the MH electrode is less than 3% after 100 cycles when lanthanum is added at 1–3 wt.%.

Keywords: Fluorination; Ni-MH battery; Hydrogen-storage alloy; Storage alloy; MH electrode; Cycle-life; Lanthanum; Metal hydride

1. Introduction

Hydrogen is a promising candidate for a clean energy source. For example, hydrogen is used as an energy-transfer medium in nickel-metal hydride (MH) batteries. The hydrogen-storage alloys used for MH electrodes in these batteries can store a great amount of hydrogen reversibly. The characteristics of the battery are mainly dependent on the properties of the MH electrode. There are two types of alloys, namely, the Zr-based AB_2 and La-based AB_5 types. The discharge capacity of Zr-based AB_2 [1] hydrogen-storage alloys is generally higher than that of the AB_5 type [2,3], but problems with cycle-life, initial activation and self-discharge still remain unresolved.

It is known that fluorination of MH electrodes improves the durability of alloys, which can increase the cycle-life of the electrodes. The detailed mechanism regarding improvement in performance due to fluorination, its effect on surface morphology and structure, hydrogen diffusion kinetics and passive oxide formation are not well understood. Suda and Liu [4] reported a performance improvement in initial activation, reaction kinetics and durability by fluorination of the surface of various hydrogen-storage alloys (AB_5, AB_2, A_2B). They investigated mainly the direct gaseous reaction between metal and hydrogen, and used a dilute acidic aqueous solution in which was dissolved special solid compound composed of F, K, and Al for fluorination.

In this study, the effects of fluorination in a fluorine-containing aqueous solution on the surface of non-stoichiometrically lanthanum-doped AB_2-type hydrogen-storage alloys, Zr–Ti–V–Mn–Ni, are investigated. On adding La to AB_2 alloys, segregated La-rich particles are formed in the AB_2 matrix and fluorides can be formed only on these particles. These characteristics were investigated by microstructure analysis and cycle test. La-rich particles of the fluorinated hydrogen-storage alloy powders are composed of a stable top-layer of an La–F compound and an Ni-rich catalytic sub-layer, which can sustain the electrochemical hydrogen absorption/desorption reaction.

2. Experimental

Hydrogen-storage alloys were prepared in an arc-melting furnace under an argon atmosphere. The alloys were crushed to particles of less than 75 μm in diameter by hydrogen absorption/desorption (note: the absorption of hydrogen causes cracks in the bulk alloy by virtue of the stresses which result from volume expansion and hydrogen embrittlement). The compositions of the alloys are listed in Table 1.

* Corresponding author. Tel.: +82-2-958-5221; fax: +82-2-958-5229.
E-mail address: hypark@kist.re.kr (H.Y. Park).

0378-7753/01/$ – see front matter
PII: S0378-7753(00)00527-9

Table 1
Composition of $Zr_{0.7}Ti_{0.3}V_{0.4}Mn_{0.4}Ni_{1.2}$ alloy samples

Sample	La content (wt.%)
M1	–
M2	1
M3	2
M4	3
M5	5
M6	10

Table 2
Model calculation of heat of formation of intermetallic compound AB of transition metals (A) with transition metals and La (B)[a]

	Zr	Ti	V	Mn	Ni	La
Zr	–	0	−5	−23	−71	+31
Ti	0	–	−3	−16	−57	+38
V	−5	−3	–	–1	−27	+50
Mn	−23	−16	−1	–	−12	+19
Ni	−71	−57	−27	−12	–	−17
La	+31	+38	+50	+19	−17	–

[a] ΔH in units of kJ g-at.$^{-1}$.

The specimen surface was characterized by scanning electron microscopy (SEM, Hitachi, S-4100), electron probe microanalysis (EPMA, Jeol, JXA-8600), and Auger electron spectroscopy (AES, Perkin-Elmer, PHI-670).

The specimens were fluorinated after polishing the as-melted alloys. Fluorination treatment was performed by stirring the MH alloy powders in an aqueous solution of KF and HF for 2 h at room temperature. The MH electrode was fabricated by pasting an alloy powder and binder (PTFE, KB, CMC) mixture on foamed nickel. A pasted-type nickel hydroxide (Tanaka) counter electrode and an Hg/HgO reference electrode were used. The electrolytic solution consisted of 30 wt.% KOH+20 g l^{-1} LiOH, and contained KF for an effectively continuous fluorination. Electrochemical characterization was performed by means of a potentiostat PAR 273A (EG&G).

3. Results and discussion

Electron micrographs and their corresponding EPMA mapping of La and F after fluorination of $Zr_{0.7}Ti_{0.3}V_{0.4}Mn_{0.4}Ni_{1.2}$ containing 3 and 5 wt.% La are shown in Fig. 1. La-rich particles approximately 5 μm in diameter are found to be dispersed throughout the surface. With increasing La content, the alloy surface hosts an increasing number of La-rich particles with a consistent diameter of 5 μm. It is presumed that the boundary between these particles and AB_2 matrices is very large.

The La-rich particles and the AB_2 matrix are expected to exist separately due to positive alloying enthalpies, as shown in Table 2 [5]. Only Ni has a negative enthalpy value with La. The analysis data of wave dispersive X-ray spectroscopy (WDS) of La-rich particles and a matrix for 3, 5, and 10 wt.% La-added alloys are shown in Table 3. It is found that the La-rich particle is an La–Ni alloy and the surface of the particle is an La–F compound with a stoichiometry of about 2.0–2.5. The surface composition of the matrix is close to the AB_2 Laves phase.

The X-ray diffraction (XRD) patterns of M1, M4, M5, and M6 alloys are given in Fig. 2. A weak La peak, at $2\theta=27^\circ$, is found only for 10 wt.% La. The XRD patterns indicate that La addition does not change the C14 Laves structure of AB_2 alloys.

The morphology of the as-cast M1 specimen is shown in Fig. 3. It is composed of dendritic matrices (A) and a second phase (B). Energy dispersive X-ray spectroscopy (EDX) composition analyses of regions A and B are given in Table 4. The composition of region A is almost the same as that of an AB_2 Laves phase. Region B is mainly composed of a Zr–Ti–Ni phase. The morphology of the as-cast M4 specimen is given in Fig. 4. The cavities formed by etching are the sites of La-rich particles which had existed before etching. Dendrite structures lose their directionality and second phases are distributed homogeneously. La-rich particles are precipitated mainly along the boundaries. La-rich

Table 3
Electron probe microanalysis of three alloys: composition (at.% and wt.%) of the La-rich and matrix phases

	M4				M5				M6			
	La-rich		Matrix		La-rich		Matrix		La-rich		Matrix	
	wt.%	at.%	wt.%	at.%	wt.%	at.%	wt.%	at.%	wt.%	at.%	wt.%	at.%
Zr	1.568	0.998	27.101	18.142	0.905	0.591	34.215	23.606	3.012	1.779	30.802	20.825
Ti	0.486	0.589	7.329	9.343	0.637	0.793	6.292	8.267	2.070	2.355	6.779	8.729
V	0.495	0.564	10.542	12.637	0.372	0.435	13.682	16.905	0.400	0.427	12.642	15.306
Mn	0.684	0.772	11.643	12.940	0.660	0.715	14.932	17.106	0.564	0.559	12.280	13.785
Ni	6.839	6.760	42.551	44.256	18.696	18.974	30.200	32.375	21.883	20.307	36.606	38.455
La	69.906	29.205	–	–	62.211	26.684	0.179	0.081	53.373	20.934	–	–
F	20.024	61.162	0.834	2.681	16.521	51.808	0.501	1.660	18.699	53.619	0.893	2.900
Total	100	100	100	100	100	100	100	100	100	100	100	100

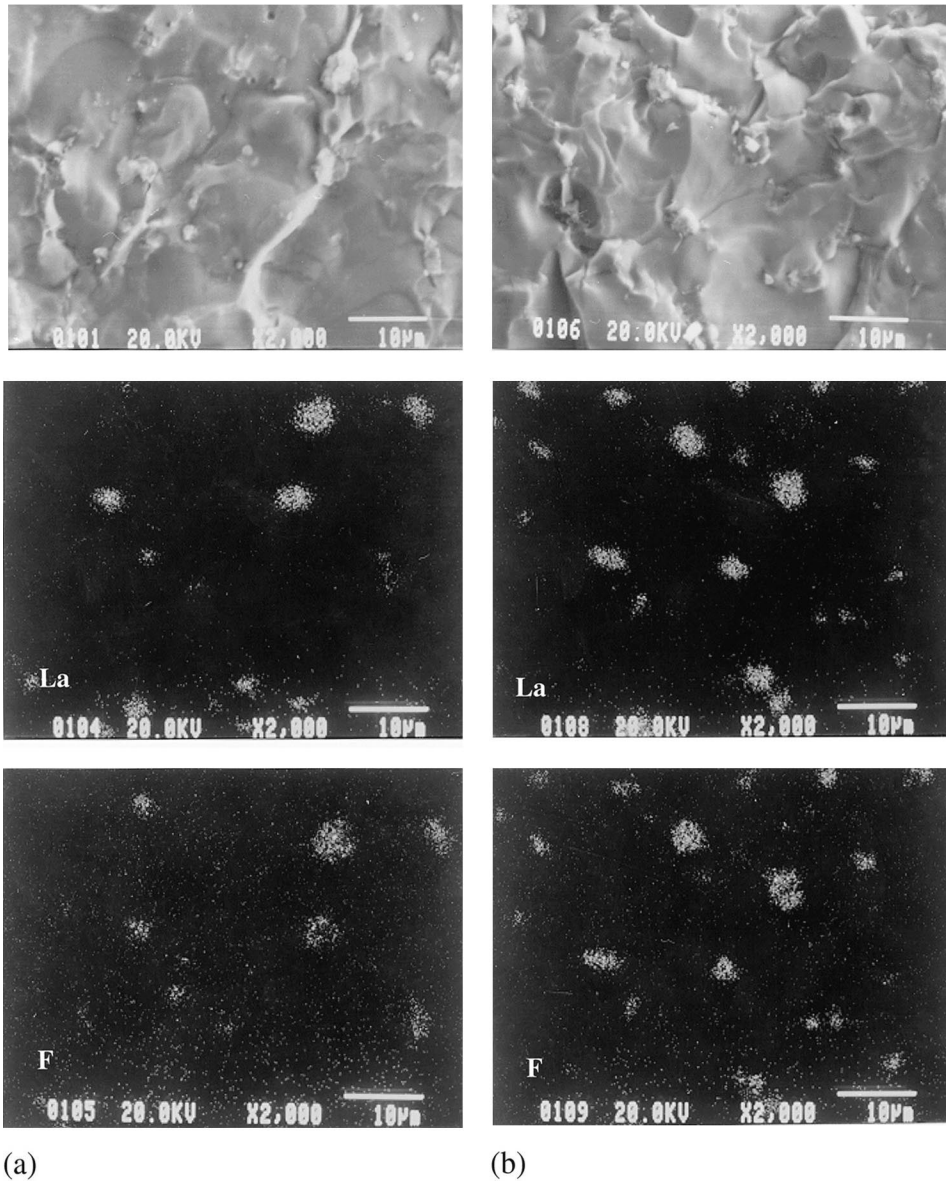

Fig. 1. Scanning electron micrograph of $Zr_{0.7}Ti_{0.3}V_{0.4}Mn_{0.4}Ni_{1.2}$ alloy surface with 3 wt.% (a) and 5 wt.% (b) La incorporation that has undergone fluorination treatment. EPMA mapping of La and F are presented for each sample.

particles also exist on the surface of crushed alloy powder. Since it is generally known that diffusion is easier through a grain boundary than through a grain, it is proposed that La-rich particles precipitated along these boundaries can act as sites of preferred hydrogen absorption. Similarly, it has been reported that hydrogen atoms penetrate through these sites easier than through a dense TiO_2 layer on the AB_2 matrix [6].

Table 4
EDX compositional analysis

Element	Content (at.%)	
	Dendrite phase (A)	Second phase (B)
Zr	26.186	26.569
Ti	9.444	16.141
V	15.381	3.836
Mn	12.661	4.816
Ni	36.328	48.638

AES depth profiles of unfluorinated and fluorinated alloy surfaces are shown in Fig. 5. In both cases, Ni increases in the sub-layer and a thin fluoride layer is formed on the top surface. It is concluded that oxygen detected deep from the surface is due to surface roughness and microcracks induced by fluorination.

The fluorination reaction is known to occur by a chemical reaction between F^- ions in equilibrium with HF/KF in the solution and lanthanum oxides via the following:

$$La_2O_3 + 6H^+ + 6F^- = 2LaF_3 + 3H_2O \quad (1)$$

$$La(OH)_3 + 3H^+ + 3F^- = LaF_3 + 3H_2O \quad (2)$$

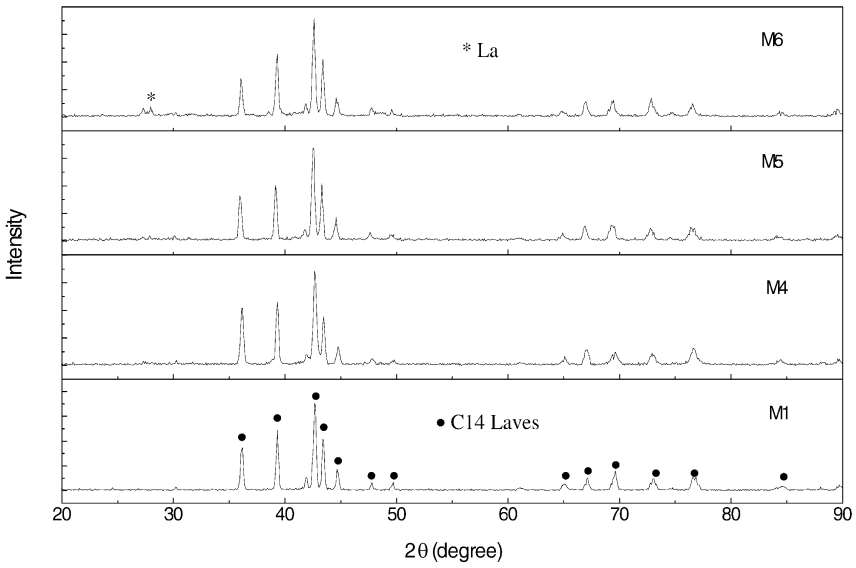

Fig. 2. X-ray diffraction analysis of four alloys.

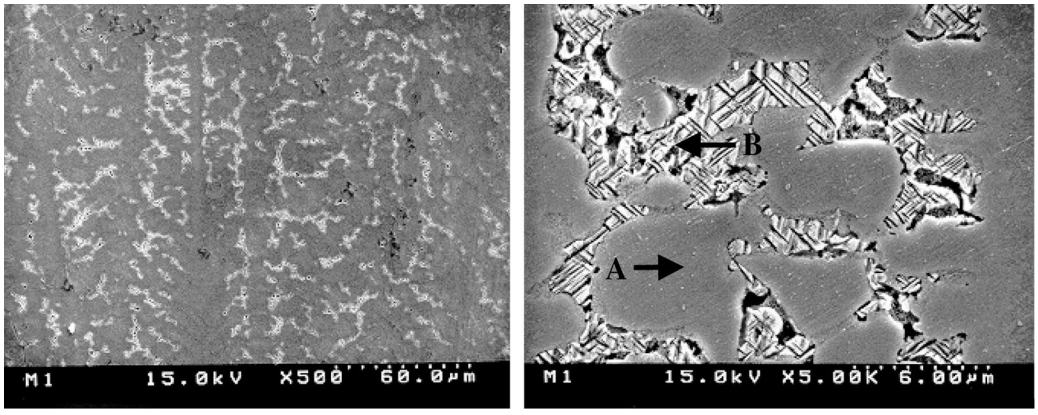

Fig. 3. Scanning electron micrograph of etched $Zr_{0.7}Ti_{0.3}V_{0.4}Mn_{0.4}Ni_{1.2}$ surface revealing regions A (dendritic matrix) and B (second phase), indicating different magnifications — (a) ×500 and (b) ×5000, respectively.

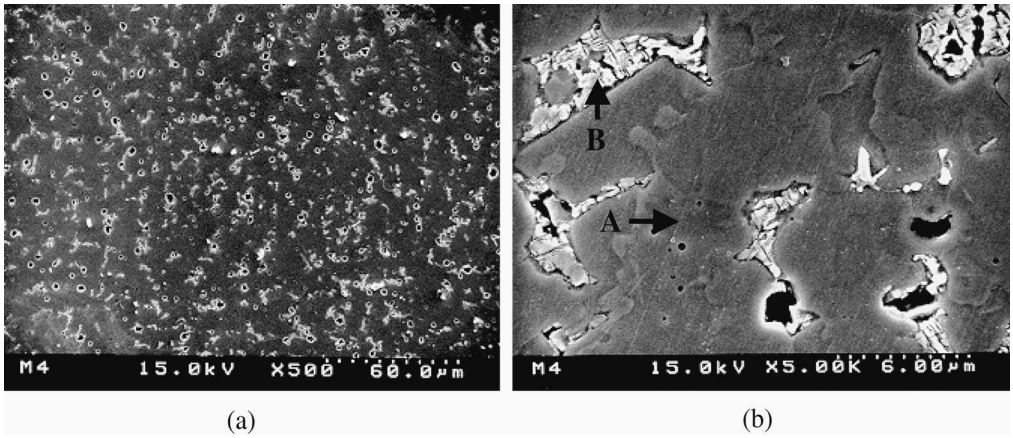

Fig. 4. Scanning electron micrograph of etched 3 wt.% La-added $Zr_{0.7}Ti_{0.3}V_{0.4}Mn_{0.4}Ni_{1.2}$ surface revealing regions A (dendritic matrix) and B (second phase). Magnification: (a) ×500 and (b) ×5000.

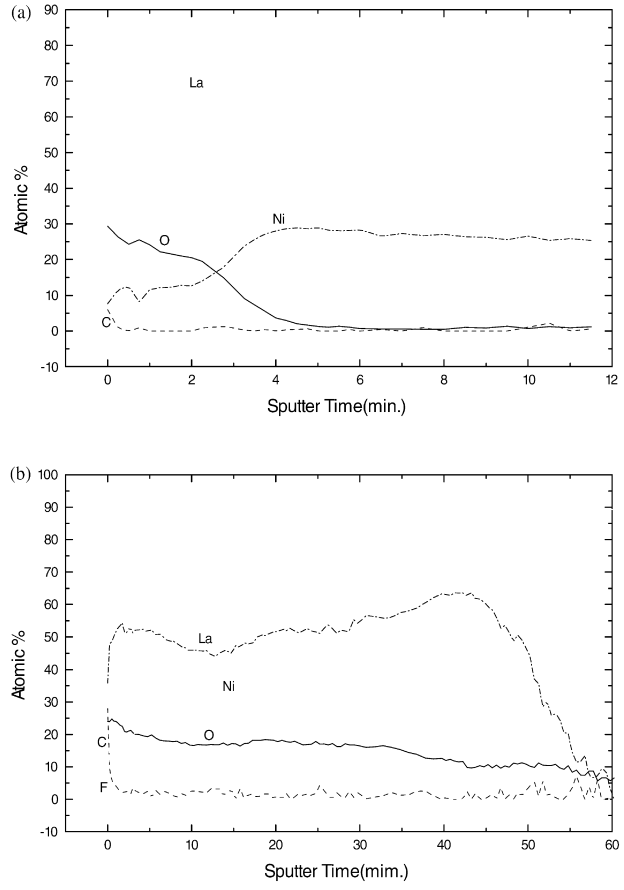

Fig. 5. Comparison of Auger electron spectroscopy of (a) untreated and (b) fluorinated La-rich particle surface of $Zr_{0.7}Ti_{0.3}V_{0.4}Mn_{0.4}Ni_{1.2}$ alloy (with 3 wt.% La incorporation).

It is suggested that the particular passive film, La–F compound, selectively allows facile penetration of hydrogen, but impedes oxygen diffusion.

The general degradation of AB_2-type hydrogen-storage alloys is due mainly to a change in the alloy surface in the electrolytic solution. It is known that, with charge/discharge cycling, the alloys are crushed by repeated expansion/contraction, and a new surface is exposed to the KOH electrolytic solution. Alloy elements are oxidized by oxygen evolved on the nickel electrode during overcharging and by an oxidation current during overdischarging. Both V and Mn dissolve in the electrolyte [7], and a TiO_2 passivation film gradually surrounds the surface. As this effect continues repeatedly, the active sites of the MH electrode are lost and the resistance increases [8]. Consequently, the MH electrode becomes degraded.

The hydriding/dehydriding reaction which occurs in La–Ni alloyed particles in an AB_2 alloy can be compared to a self-restoring mechanism for $LaNi_5$ systems, as described by Schlapbach and coworkers [9,10]. In an $LaNi_5$ system, La segregates to the surface and oxidizes to form La_2O_3-type passive films, while Ni remains in a metallic or Ni-rich precipitated form and catalyzes the hydriding/dehydriding reaction. The Ni-rich region, however, can also oxidize, and eventually cause alloy degradation.

A fluorinated product precipitated on the surface is thus critical in forming a protective film which preserves the La-rich particle. When fluorinated, La-rich particles with an La–F compound top layer can function as easy hydrogen penetration sites whilst protecting against surface oxidation. Thus, degradation of MH electrodes can be prohibited.

Charge/discharge curves are given in Fig. 6 for both fluorinated and unfluorinated MH electrodes, namely, La-

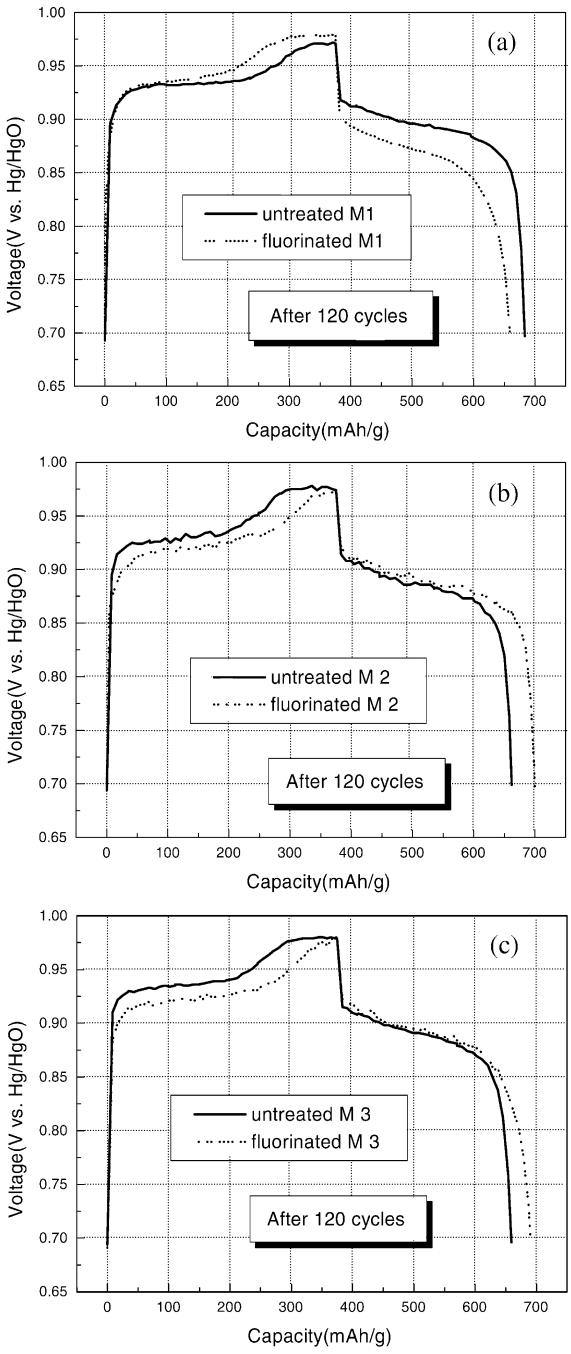

Fig. 6. Comparison of charge/discharge characteristic curves of F-treated and untreated alloys — (a) M1; (b) M2; (c) M3.

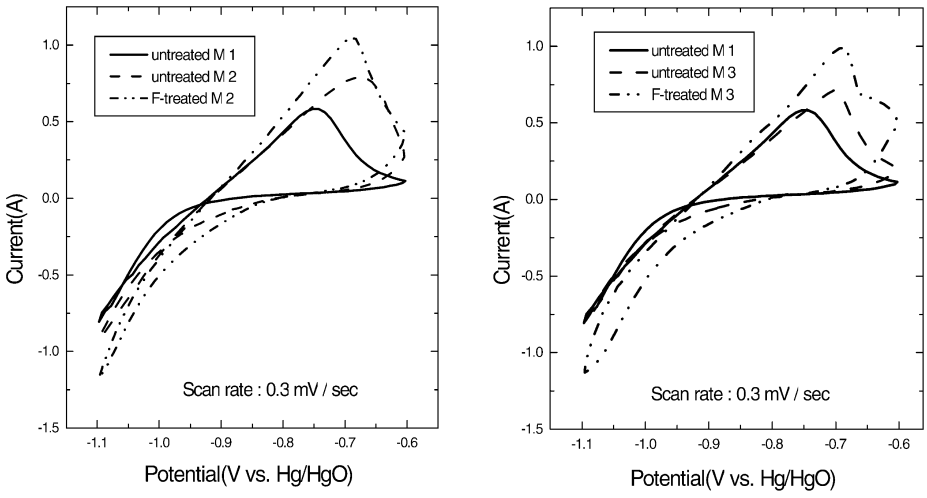

(a) M1 and M2 (b) M1 and M3

Fig. 7. Cyclic voltammograms of MH electrodes (after 120 cycles).

free M1, 1 wt.% La-added M2, and 2 wt.% La-added M3, after 120 cycles. The drop in voltage during discharge is about 0.05 V for most of the electrodes, and the charge/discharge characteristics of La-added types are distinguishable from those of La-free alloys. In the case of M1, the charge potential is increased and the discharge potential is decreased by fluorination; the potential difference between the charge/discharge plateau, i.e., polarization (overpotential), is also increased. By contrast, the polarization characteristics of M2 and M3 are improved by fluorination. Yan et al. [11] reported that the polarization characteristics of La-free $Zr_{0.5}Ti_{0.5}V_{0.75}Ni_{1.5}$ alloy are improved by fluorination, because the kinetics of hydrogen absorption/desorption are improved by the formation of microcavities and by an increase in the specific surface area. Since this differs from the results for M1, further examination of this sample is required.

Cyclic voltammograms for unfluorinated M1, M2, M3 electrodes and fluorinated M2, M3 electrodes after 120 cycles are shown in Fig. 7. The fluorinated electrodes exhibit high hydrogen absorption/desorption currents and low overpotentials. The electrode characteristics are therefore improved by fluorination of La-added alloys.

Potential versus current plots for a current swept from 0 to 100 mA at a rate of 0.333 mA s^{-1} for M2 alloy cells after 100 cycles are presented in Fig. 8. The slopes, analogous to resistance, are 0.4455 V A^{-1} for unfluorinated and 0.3420 V A^{-1} for fluorinated alloy. The lower slope shows that fluorination of La-added alloy maintains fast and continuous hydrogen oxidation and reduction. In addition, the resistance value of fluorinated M2 for hydrogen reduction is lower than the unfluorinated M1 at similar comparing potential levels.

From the results of Figs. 7 and 8, it is clear that a continuous hydrogen penetration is possible through La-rich regions with a fluorinated surface, although the AB_2 matrix is degraded by surface oxidation.

The cycling performance of fluorinated and unfluorinated electrodes is shown in Fig. 9. Fluorinated electrodes are more stable than untreated electrodes, especially when the La content is 1–3 wt.%. The maximum discharge capacity is ~340 mA h g^{-1}. Above 5 wt.% La, there appears to be no effect on both the cycling performance and the discharge capacity due to the loss of active materials. Furthermore, in the case of M1 alloy, the discharge capacity of the fluorinated electrode decreases more rapidly than that of the unfluorinated counterpart. It is speculated that fluorination in the absence of La has no effect and the alloy corrodes continuously in the presence of F^- ions.

A proposed schematic diagram of the fluorinated surface structure of La-added alloy is illustrated in Fig. 10. It is assumed that La-rich particles on the AB_2 alloy protect the

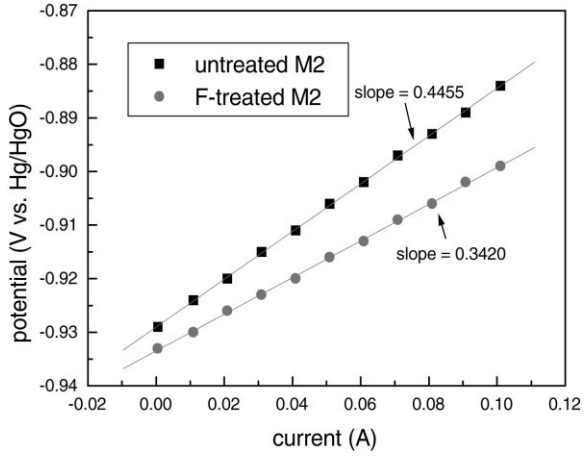

Fig. 8. Potential vs. current plots for M2 alloy cells (0.333 mA s^{-1} rate).

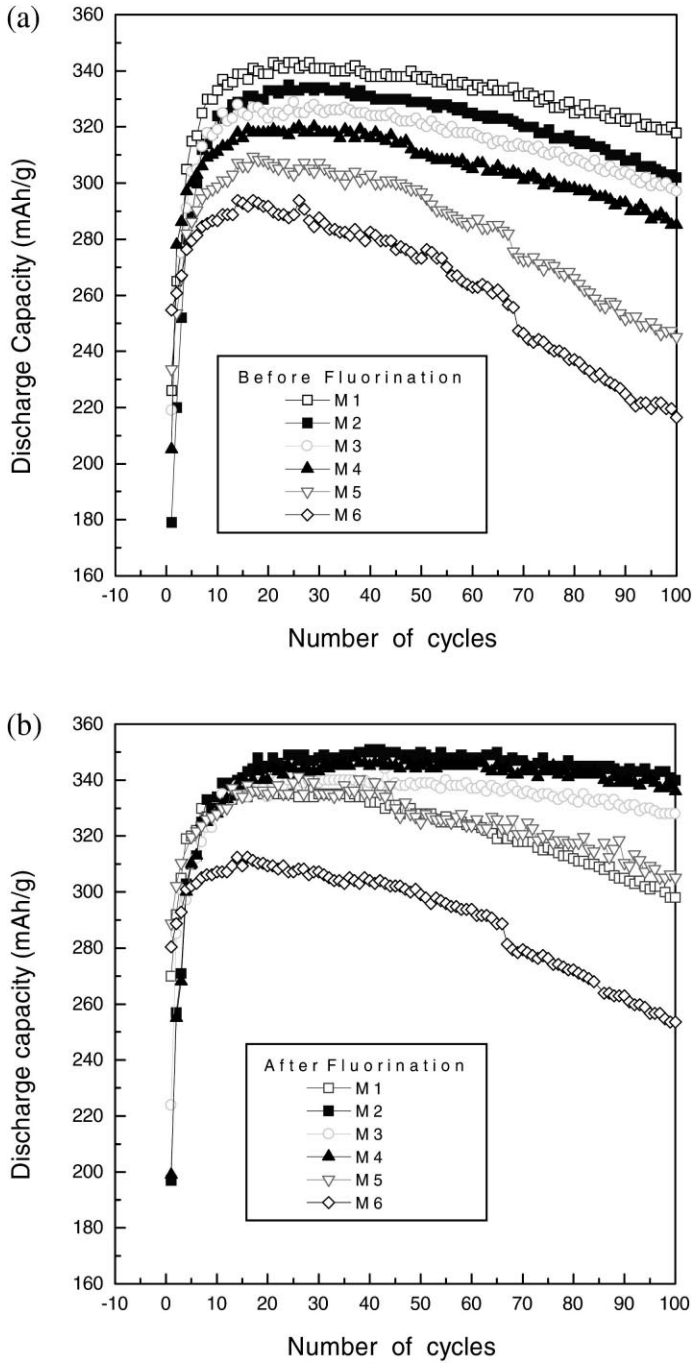

Fig. 9. Discharge capacity cycle performance of (a) untreated alloys and (b) fluorinated alloys.

surface from oxidation and form a stable La–F compound as a pathway for facile hydrogen penetration. Although oxide layers (e.g. TiO_2 or ZrO_2) on the AB_2 matrix impede hydrogen penetration, the Ni-rich sublayer on the La-rich particles acts as a catalyst for hydrogen dissociation and H atoms diffuse easily through the boundary between the La-rich particle and the AB_2 matrix and through the dendritic boundary under the La-rich particle.

4. Conclusions

The cycle performance of fluorinated La-added AB_2 alloys has been studied. The fluorination of La-added AB_2 alloys imparts significant improvements on the cycle-life of the MH electrode. La, especially fluorinated, is proposed to provide a protective shield against oxidation, as well as an easy hydrogen pathway.

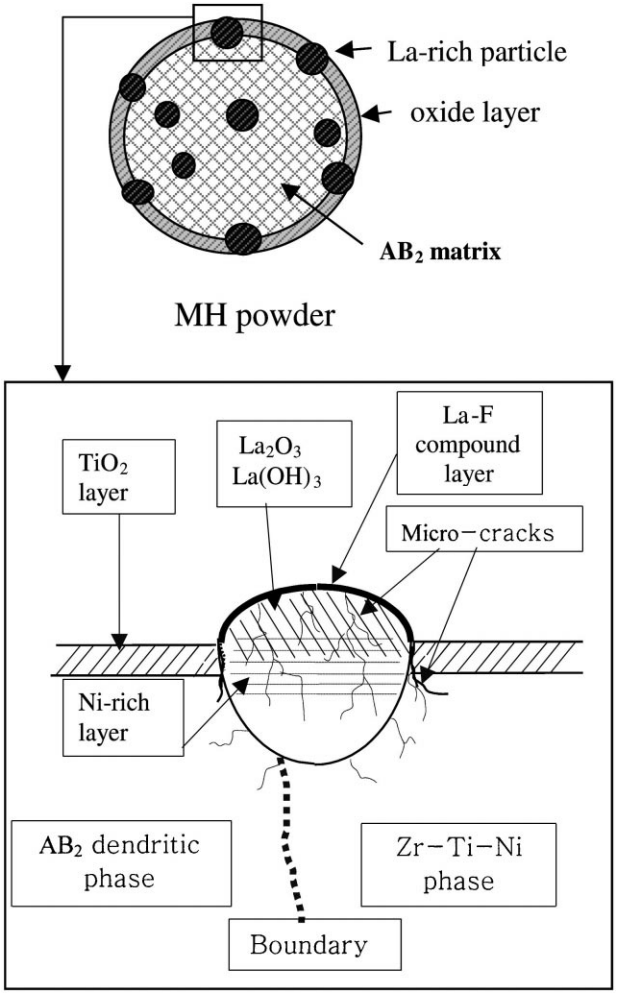

Fig. 10. Schematic diagram of La-rich region on the surface of AB_2 alloy.

SEM and EDX of the etched alloy reveals at least two different phased regions, composed of dendritic matrices and Zr–Ti–Ni rich second phases. The boundaries of these regions are interconnected with La-rich particles. It is therefore proposed that hydrogen enters through the fluorinated La window and diffuses along the dendritic boundaries at a much faster rate than through the AB_2 matrix with an oxide film.

The following specific observations are noted:

1. La is not soluble in a Laves phase $Zr_{0.7}Ti_{0.3}V_{0.4}Mn_{0.4}Ni_{1.2}$ hydrogen-storage alloy but forms a separate La-rich particle on the dendrite boundary through which H atoms can diffuse easily.
2. A stable La–F compound is formed on the surface of La-rich particles by fluorination treatment, while a stable fluoride film does not form on the AB_2 matrix.
3. La-rich particles have a surface structure which is composed of a protective La–F compound top-layer and a catalytic Ni-rich sub-layer which acts as a site for easy hydrogen penetration.
4. Fluorination of La-added MH improves the polarization characteristics of the electrode for charging and discharging.
5. Fluorination prohibits the degradation of the MH electrode and increases its cycle-life, especially when the La content is in the range of 1–3 wt.%.

References

[1] K. Hong, M. Fetcenco, S. Venkatesan, B. Reichman, J. Power Sources 12 (1988) 411.
[2] A.H. Boonstra, G.J.M. Lippits, T.N.M. Bernards, J. Less-Common Metals 155 (1989) 119.
[3] T. Sakai, H. Hazama, H. Miyamura, N. Kuriyama, A. Kato, H. Ishikawa, J. Less-Common Metals 172–174 (1991) 1175.
[4] F.-J. Liu, S. Suda, J. Alloys and Compounds 231 (1995) 742.
[5] A.R. Miedema, Philips Tech. Rev. 36 (1976) 217.
[6] F.-J. Liu, G. Sandrock, S. Suda, J. Alloys and Compounds 231 (1995) 392.
[7] J.S. Kim, Ph.D. Thesis, Seoul National University, 1995.
[8] H.H. Lee, Ph.D. Thesis, KAIST, 1996.
[9] H.C. Siegmann, L. Schlapbach, C.R. Brundle, Phys. Rev. Lett. 40 (1978) 972.
[10] L. Schlapbach, A. Seiler, H.C. Siegmann, T.V. Waldkirch, P. Zurcher, Int. J. Hydrogen Energy 4 (1979) 21.
[11] D.-Y. Yan, Y.-M. Sun, S. Suda, J. Alloys and Compounds 231 (1995) 387.